Spatio-temporal variations of nitrate pollution of groundwater in the intensive agricultural region: hotspots and driving forces

Xueqiang Zhu[1, 2,3], Peng Miao[1, 2], Wanhong Li[1, 2], Mingxia Yang[1, 2], Lei Wang[3], Zhujun Chen[1, 2]*, Jianbin Zhou[1, 2]*

[1]*College of Natural Resources and Environment, Northwest A&F University, Yangling, Shaanxi 712100, China*

[2]*Key Laboratory of Plant Nutrition and the Agri-environment in Northwest China, MOA, Yangling, Shaanxi 712100, China*

[3]*British Geological Survey, Keyworth, Nottingham NG12 5GG, UK*

Corresponding author:

Jianbin Zhou, Zhujun Chen

Email: jbzhou@nwsuaf.edu.cn, zjchen@nwsuaf.edu.cn

Abstract:

Nitrate (NO_3^-) pollution of groundwater is a persistent and widespread problem worldwide, particularly in intensive agricultural regions with high nitrogen (N) surplus. Identifying spatio-seasonal variations, drivers and sources of NO_3^- in groundwater is key to controlling this pollution. In this study, we monitored 175 wells in areas with different irrigation practices (dryland, well irrigation and canal irrigation) in an intensive apple-planting region over a year (September 2020-October 2021) in the southern Loess Plateau, China. The integration of hydrochemical analysis, deep soil profiles, NO_3^- isotopic composition and a Bayesian isotope mixing model (SIAR) was used to identify the hotspots and hot moments of groundwater NO_3^- pollution, and main NO_3^- sources. The results showed that average NO_3^- concentrations of three regions gradually decreased from north to south, following the order of dryland region (9 mg NO_3 L^{-1}) < well irrigation region (23 mg NO_3 L^{-1}) < canal irrigation region (94 mg NO_3 L^{-1}), and orchard > residential area ≈ cereal land. In the study region, 44% of groundwater exceeded the drinking standard of the World Health Organization (50 mg NO_3 L^{-1}). The intensive apple planting in the canal-irrigated regions has caused groundwater NO_3^- pollution, and changed hydrochemical types from HCO_3^-Ca·Mg to SO_4·Cl·NO_3-Ca·Mg. In the canal irrigation region, NO_3^- in the vadose zone has migrated to groundwater. The hotspots of groundwater NO_3^- pollution (NO_3^- vulnerable zones) were identified at low-altitude loess tableland and alluvial plains with canal irrigation. Irrigation and precipitation accelerated soil NO_3^- deep migration. The hot moments of NO_3^- pollution in the irrigated region was the period from the wet season to the dry season; and the "hidden reactive N pool" in the deep vadose zone (>2 m) caused a time lag of NO_3^- reaching into groundwater. Chemical N fertilizer and manure N applied in apple orchards were the main contributing sources of groundwater NO_3^- pollution in the apple-planting region. Our study highlights the significant effect of apple-planting industry development on groundwater quality.

Keywords: Apple-planting region, Nitrate pollution, Spatio-seasonal variations, Source identification

1. Introduction

Groundwater is the main water source for agriculture, daily life, industry, and ecology in arid, semi-arid and sub-humid regions, where surface water resources are scarce (Famiglietti, 2014; Ravindra et al., 2022). With the development of agricultural and industrial production, global groundwater quality is threatened by anthropogenic activities, especially polluted by nitrate (NO_3^-) due to high N surplus in the intensive agricultural region (Burow *et al.*, 2010; Rao et al., 2021; Steffen *et al.*, 2015). Long-term exposure to NO_3^- concentrations exceeding World Health Organization (WHO) allowable drinking standard (50 mg NO_3 L^{-1}) (WHO, 2017), poses severe hazards to human health, including methemoglobinosis, digestive system cancer, and blue baby syndrome (Bryan and Loscalzo, 2011; Willett *et al.*, 2019). Therefore, the assessment of groundwater NO_3^- pollution is of practical significance for an intensive agricultural region with a high N surplus.

Groundwater NO_3^- concentrations, which have high spatial and seasonal variation, are controlled by many driving factors, such as the thickness of the vadose zone, land-use types, agricultural water management, and N surplus (Cameira *et al.*, 2021; Gao *et al.*, 2021a; Gu *et al.*, 2013). The vadose zone provides a large space for NO_3^- accumulation and delays the migration of legacy NO_3^- from the root zones to aquifers (Weitzman *et al.*, 2022). NO_3^- time lags include biogeochemical lag and hydrologic lag in the vadose zone and aquifer (Van Meter *et al.*, 2018; Basu *et al.*, 2022). Seasonal variations in groundwater NO_3^- concentrations reflect agricultural management practices (fertilization and irrigation) and precipitation in both dry and wet seasons (Meghdadi and Javar, 2018; Rotiroti *et al.*, 2019). The NO_3^- time lags also affect the seasonal variations in groundwater NO_3^- concentrations. Therefore, understanding the spatio-seasonal variations and drivers of groundwater NO_3^- concentrations and identifying the hotspots and hot moments of groundwater NO_3^- pollution are important not only for establishing effective water quality management practices, but also for designating the NO_3^- vulnerable zones.

The sources of groundwater NO_3^- mainly include chemical fertilizer (CF), soil organic N (SN), manure and sewage (M&S), and atmospheric deposition (AD) (Xue *et al.*, 2009; Meghdadi and Javar, 2018). Identifying the sources of groundwater NO_3^- is of primary importance for understanding the mechanism of NO_3^- loss in an ecosystem. Different NO_3^- sources have different stable isotope features (Kendall *et al.*, 2007; Xue *et al.*, 2009). Hence, the natural abundances of ^{15}N and ^{18}O of groundwater NO_3^- can be used to identify the NO_3^- sources of groundwater (Xue *et al.*, 2009; Gao *et al.*, 2021a; Xiao et al., 2022). However, the use of stable isotope analysis alone cannot always provide conclusive information due to the overlapping isotopic values and isotope feature changes caused by different biogeochemical processes (Xue *et al.*, 2009). In addition, the pollutants from human activities are characterized as being rich in K^+, Mg^{2+}, SO_4^{2-}, Cl^-, and NO_3^- in groundwater (Meghdadi and Javar, 2018; Rao et al., 2022). The relationships between Cl^- and NO_3^-/Cl^- ratio have been used to identify the potential sources of NO_3^- in groundwater (Meghdadi and Javar, 2018; Torres-Martínez *et al.*, 2021). Therefore, an integration of dual isotope analysis, hydrochemical analysis and a Bayesian isotope mixing model (SIAR) is helpful for the source identification of groundwater NO_3^-.

Dramatic land-use change has occurred in China since1980s. Large areas of cereal lands have been converted to cash crops, such as horticultural crops (e.g., orchards and vegetable fields).

The application rates of N fertilizers in horticultural crops are usually high compared to cereals, thus making the horticultural systems the hotspots of N surplus and N losses (Zhu *et al*., 2022a). The Loess Plateau (LP) in China, the largest area covered by loess deposit up to 350 m deep (Zhu *et al.*, 2018), has become the largest intensive apple-planting region (1.2×10^6 ha) in the world due to the abundant light and heat resources (FAOSTAT, 2019; Li *et al.*, 2018). Overuse of N fertilizers (manure and chemical fertilizer) is common in the apple orchard on the LP. High N fertilizer input leads to surplus N, which is mainly accumulated in the soil profile as NO_3^- due to strong nitrification potential and weak denitrification of soils (Zhu *et al.*, 2021; Zhu *et al.*, 2022b). However, the effect of intensive apple planting on NO_3^- pollution of groundwater is not well understood. The orchards of the northern apple-planting region on the LP are usually rain-fed, and the south orchards are irrigated by water from wells or canals (Zhu *et al.*, 2022b) (Fig. 1). Compared with canal irrigation, groundwater/well irrigation is used in high-elevation orchards, and the irrigation rate is usually low due to high groundwater-pumping costs. Most studies mainly focused on the orchard in rain-fed regions and showed that NO_3^- mainly accumulates in 0-6 m soil layer with little influence on regional groundwater (Huang *et al.*, 2018; Liu *et al.*, 2019; Zhu *et al.*, 2021). Nevertheless, few studies have reported the vertical distribution and seasonal variation of NO_3^- in the deep vadose zone in the irrigated regions; and the spatio-seasonal variations, drivers and sources of groundwater NO_3^- are unknown. We hypothesized that serious NO_3^- pollution of groundwater in the canal irrigation region may have occurred due to high water input and long-term overuse of N fertilizers.

Therefore, we collected groundwater samples from the typical apple product counties in the south LP over a year. The objectives of this study are to (1) evaluate spatio-seasonal variations of groundwater NO_3^- concentrations; (2) find out hot spots and hot moments of groundwater NO_3^- pollution; and (3) identify the main sources of groundwater NO_3^- using hydrochemical analysis, isotope analysis and SIAR.

2. Materials and methods

2.1 Study region

The study region is located in the south of the Loess Plateau in Shaanxi, China (N34°07′10″–38°14′53″, E104°58′04″–112°03′10″); and the topography slopes from north to south with altitudes ranges from 290 m and 2700 m in the study region (Fig. 1). The mean annual temperature and precipitation in the region is 10 °C and 520 mm, respectively. More than 60% of annual precipitation occurs between July and September. The average monthly precipitation of five meteorological monitoring stations during the study period is shown in Fig. 2. The apple planting has developed very fast since the 1990s due to the high profits compared with that from cereal lands. Apple orchards in the north are rain-fed without irrigation, i.e., the dryland region. Orchards in the south are canal irrigation, and the irrigation water is mainly from the reservoirs (19 mg NO_3 L^{-1}) and Wei River (25 mg NO_3 L^{-1}), i.e., the canal irrigated region. The orchards between the dryland region and canal-irrigated region are irrigated with water from wells, i.e., the well-irrigated region (Fig. 1d). Compared with canal irrigation (450 mm yr^{-1}), the annual irrigation amount in the well-irrigated region (< 300 mm yr^{-1}) is lower due to high costs for groundwater pumping. Chemical fertilizer N and manure N are added to apple orchards with an average of 1200 kg N ha^{-1} yr^{-1} (Chen et al., 2019), and manure N accounts for 25% of annual N fertilizer input (Wang et al., 2013a). In the dryland region, winter wheat-summer fallow tillage mode is used, and the N fertilizer application rate is about 180 kg N ha^{-1}. In the irrigation region with winter wheat-summer maize tillage mode, the N fertilizer application rate is about 435 kg N ha^{-1} (Gao et al., 2021b).

2.2 Hydrogeology

Quaternary sediments including alluvial, alluvial-pluvial, and eolian cover the study region; and the unconfined aquifers are continuously distributed. The main geomorphology includes loess tableland, mountains, and the alluvial plain. The depths of water tables in the alluvial plain are usually less than 20 m, while it is deep in loess tableland, and even more than 100 m in the drylands to the north (http://www.mwr.gov.cn). Precipitation and irrigation are the main recharge sources for the groundwater, while groundwater discharge occurs by evapotranspiration, artificial extraction and lateral outflow in this region.

The groundwater generally flows from the loess tableland or mountains (high altitude) in the north to the alluvial plain or Wei River Plain (low altitude) (Fig. 1 and Fig. S1). The phreatic water in this area is mainly unconsolidated sediments pore water. In the study region, which has relatively extensive river systems, groundwater is pumped for drinking and irrigation. The Yellow River runs through the study area, and the Wei River is in the south of this region (Fig. 1).

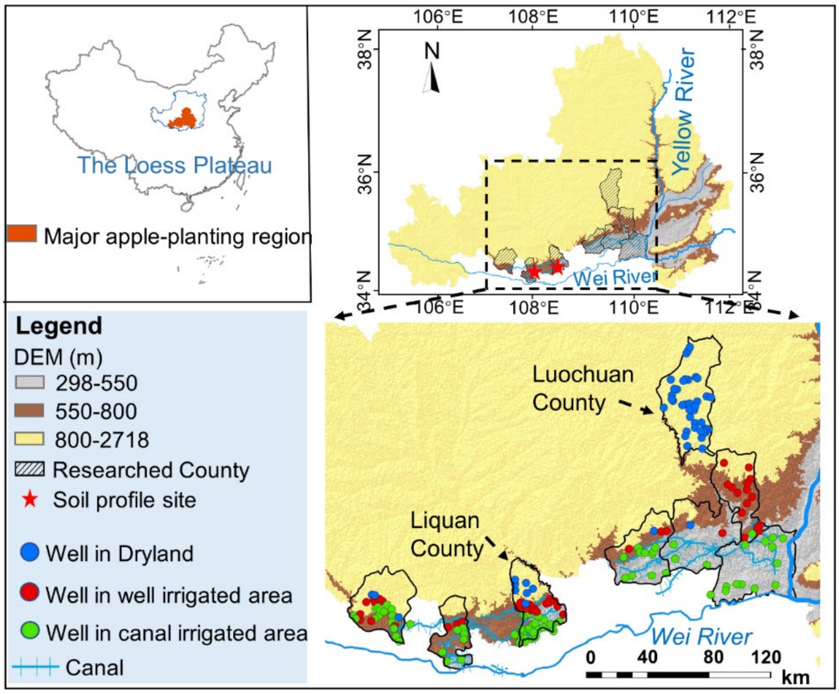

Fig. 1 Spatial distribution of apple-planting region and sampling sites on the LP.

2.3 ***Study methods***

To identify the hotspots, hot moments and drivers of groundwater NO_3^- in the study region, we chose three regions based on irrigation types from north to south i.e., dryland region, well-irrigated region and canal irrigated region, including eight counties (Luochuan, Chengcheng, Pucheng, Fuping, Dali, Liquan, Fufeng, and Fengxiang countries (Fig. 1). 175 wells were monitored from September 2020 to October 2021 for orchard/cereal lands (Fig. 1 and Fig. 2). The groundwater samples were taken four times from the wells for domestic and agricultural uses, including September 2020 (wet season), December 2020 and March 2021 (dry season), and October 2021 (wet season). The wells were pumped continuously for at least 10 minutes before collecting groundwater samples. Dissolved oxygen (DO) was measured *in-site* using a portable instrument of JPB-607A type (Leici Corp., Shanghai, China). Samples were filtered through 0.45 μm cellulose membranes and kept at 4 ℃.

To explore the seasonal variations in the vertical distribution of NO_3^- in the vadose zone

(NO_3^- profile), we took soil profile samples from topsoil to water tables in three apple orchards (AO_1, AO_2 and AO_3), of which AO_1 was sampled two times, i.e., in April 2021 (dry season) and October 2021 (wet season) (Fig. 7a and b). AO_2 (Fig. 7c) and AO_3 (Fig. 7d) were sampled in October 2021 (wet season). We drilled a borehole in the center of the orchard (approximately 1 m away from the tree trunk) with (add the name of the driller??), collecting soil samples at 0.2 m intervals. Soil moisture and NO_3^- contents were measured. The precipitation data (from September 2020 to October 2021) were collected from the China Meteorological Data Sharing Service System (http://cdc.cma.gov.cn/) (Fig. 2).

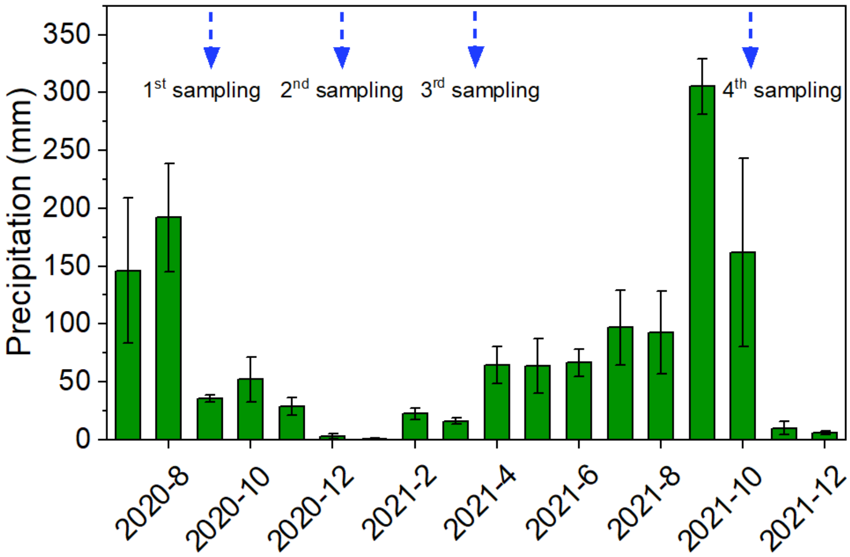

Fig. 2 Sampling time and average monthly precipitation during the whole apple orchard fruit-production cycle. Bars indicate the standard deviation of annual precipitation in five meteorological monitoring stations in the study region.

2.4 *Soil and groundwater samples analysis*

The soil gravimetric water content (θ) was measured by drying a minimum of 30 g of soil at 105 °C for 24 hours. The NO_3 concentration of fresh soil was measured by the KCl extraction method (1 mol L^{-1} KCl; 1:10, soil/solution). The extractant was measured by a continuous flow analyser (AutoAnalyzer 3, Branand Luebbe, Germany). NO_3 concentrations of the soil water (mg NO_3 L^{-1}) were calculated according to Huang *et al.* (2018).

Major cations (K^+, Na^+, Ca^{2+} and Mg^{2+}) concentrations were measured using atomic absorption spectrophotometry (Z-2000, ICP-AES, Japan). HCO_3^- and CO_3^{2-} concentrations were measured by titration (0.01 mol/L H_2SO_4). SO_4^{2-} concentration was measured by turbidimetry (Sörbo, 1987; Krug *et al.*, 1977). Silver nitrate titration was used to analyze Cl^- concentration, and NO_3^- concentration was measured by a continuous flow analyser. pH and electrical conductivity (EC) were measured using a pH meter of DELTA320 type (Mettle Corp., Greifensee, Switzerland) and a conductivity meter of DDS-307A type (Leici Corp., Shanghai, China), respectively. The charge balance error (%CBE) was calculated for all water samples, and the %CBE values within the acceptable limit of ±5% were used as indicators of analysis accuracy.

The $\delta^{15}N$-NO_3^- and $\delta^{18}O$-NO_3^- values of groundwater NO_3 were determined using the bacterial denitrification method (Sigman *et al.*, 2001). The $\delta^{15}N$ and $\delta^{18}O$ analysis of the produced N_2O was operated by a trace gas preparation unit (Gas-BenchII, Thermo Fisher, USA) coupled to an isotope ratio mass spectrometer (MAT253, Thermo Fisher, USA). The isotope ratios were corrected according to the international standards USGS32 ($\delta^{15}N$ = +180‰, $\delta^{18}O_{VSMOW}$ = +25.7‰) and USGS34 ($\delta^{15}N$ = −1.8‰, $\delta^{18}O_{VSMOW}$ = −27.9‰). The measurement errors for $\delta^{15}N$-NO_3^- and $\delta^{18}O$-NO_3^- are less than 0.5‰ and 1‰, respectively. Isotope analyses were operated at the Analyzing and Testing Center of the Third Institute of Oceanography, Ministry of Natural Resources, China.

2.5 *Calculation approach*

The nitrate accumulation amount (kg N ha^{-1}) in the soil profiles was calculated for each sampling site as follows (Zhu et al., 2022b):

$$\text{Nitrate accumulation amount} = SBD \times C \times d \times 10^{-1} \quad (1)$$

where SBD is the soil bulk density (g cm^{-3}), C is the soil nitrate content (mg N kg^{-1}), d is the thickness of the soil layer (cm), and 10^{-1} is the conversion factor.

To estimate the contribution of the different NO_3^- sources in the region, the SIAR mixing model was used. The details are provided by Xue *et al.* (2012).

$\delta^{15}N$ and $\delta^{18}O$ values (‰) from four potential NO_3^- sources, i.e., atmospheric N deposition (AD), soil N (NS), chemical N fertilizer (NF), and manure N (M), were used as specific isotope values (Table 1) to identify the main sources of the groundwater NO_3^-.

Table 1 $\delta^{15}N$ and $\delta^{18}O$ values (‰) of different potential NO_3^- sources in groundwater

Sources	Mean $\delta^{15}N$	SD $\delta^{15}N$	Mean $\delta^{18}O$	SD $\delta^{18}O$
AD[a]	-2.5	11	67.4	10
NF[b]	0.9	2	1.5	1.4
NS[c]	5	1.5	-2.7	4.4
M[d]	16.3	5.7	5	2.7

Note: SD means standard deviation. [a]Data obtained from Gao *et al.* (2021a); [b]Data, [c]Data and [d]Data obtained from Cao *et al.* (2021) and Gao *et al.* (2021a).

2.6 *Analysis*

The analysis of variance (ANOVA) was operated in SPSS 19.0 (IBM Corp., Armonk, USA). Regression analysis was used to analyse the relationship between NO_3^- concentration and controlling factors. The significant differences were analysed by Duncan's multiple range tests at $p < 0.05$ and $p < 0.01$.

3. Results

3.1 Hydrochemical characteristics of the groundwater

High coefficients of variation (CVs) of groundwater physicochemical characteristics were found in the study region (Table 2). Average cation concentrations in the groundwater followed the order of $Ca^{2+} > Na^{+} > Mg^{2+} > K^{+}$ in the dryland region, and $Na^{+} > Ca^{2+} > Mg^{2+} > K^{+}$ in the irrigation region, whereas average anion concentrations exhibited the following order: $HCO_3^- > SO_4^{2-} > Cl^- > NO_3^-$ in the study region. Average EC, K^+, Na^+, Cl^-, SO_4^{2-}, and NO_3^- values of groundwater in the different regions followed the order of canal irrigation > well irrigation > dryland (Table 2). Average NO_3^- concentrations of groundwater in the dryland region, well-irrigated region and canal-irrigated region were 9 mg NO_3 L^{-1}, 23 mg NO_3 L^{-1} and 94 mg NO_3 L^{-1}, respectively (Table 2). The NO_3^- concentrations of ~64% of groundwater samples in the canal-irrigated region were higher than WHO allowable drinking water standard (50 mg NO_3 L^{-1}) (WHO, 2017); for dryland region and well-irrigated region, it was 2% and 9%, respectively.

The major ions of groundwater are shown in a piper diagram (Fig. 3). The groundwater types in the dryland region mainly belong to HCO_3-Ca·Mg types, and those in the well-irrigated region were the HCO_3-Ca·Mg and HCO_3-Na types, while the groundwater types in the canal irrigated region were more complex and can be classified into four types, i. e., SO_4·Cl·NO_3-Ca·Mg, HCO_3-Ca·Mg, HCO_3-Na and SO_4·Cl·NO_3-Na (Fig. 3).

Table 2 The values of the main physicochemical characteristics of groundwater samples in the study region (mean±SD)

Category	EC (μs/cm)	pH	Ca^{2+} (mg/L)	Mg^{2+} (mg/L)	K^{+} (mg/L)	Na^{+} (mg/L)	SO_4^{2-} (mg/L)	Cl^{-} (mg/L)	NO_3^{-} (mg/L)	HCO_3^{-} (mg/L)	Dissolved oxygen (DO) (mg/L)
Dryland region (n=48)	490±179	8±0.16	51±18	21±6	1.2±1.5	32±36	33±23	14±15	9±10	266±73	7.2±1.7
Well irrigation region (n=46)	863±345	7.84±0.27	56±34	31±14	2.2±1.7	109±85	65±49	44±27	23±19	423±150	6.6±1.9
Canal irrigation region (n=80)	1472±1308	7.78±0.38	64±46	62±37	2.3±2.5	153±127	148±114	98±96	94±89	432±154	5.8±1.8
Coefficient of variation (%)	96	3.5	64	75	103	102	102	126	140	40	29

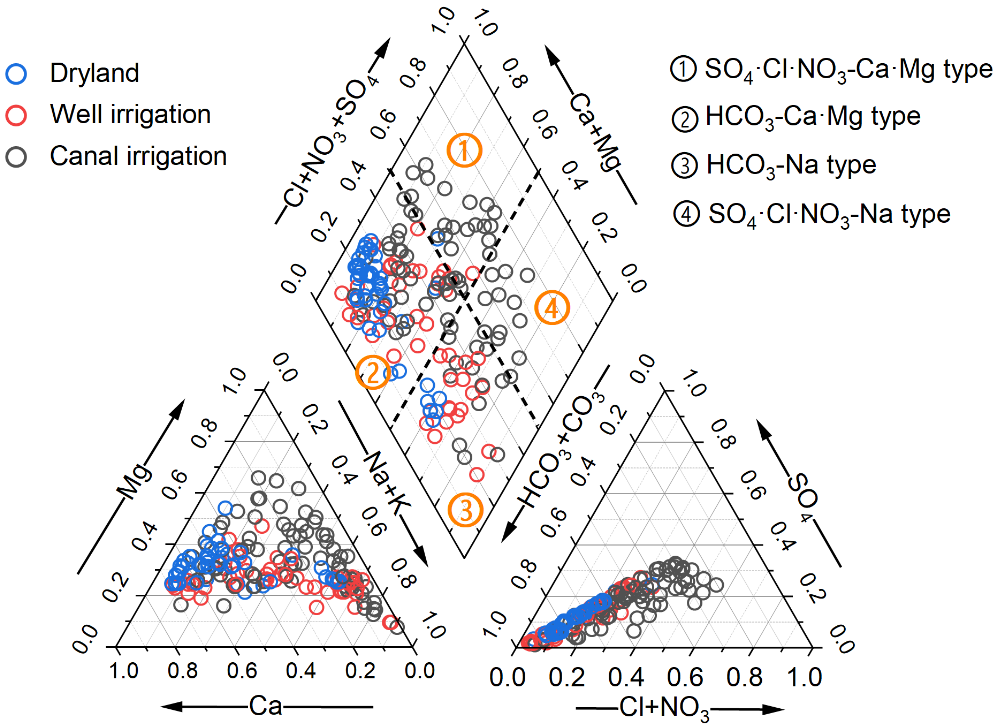

Fig. 3 Piper diagram of groundwater in different regions

3.2 Spatio-temporal variations and drivers of groundwater NO_3^- concentration

3.2.1 Spatial variations and drivers of groundwater NO_3^- concentration

Groundwater NO_3^- concentrations significantly increased from north to south of the study region during the sampling periods; high NO_3^- concentrations of groundwater were found in the low-altitude regions (Fig. 4a). The NO_3^- concentrations of groundwater significantly decreased exponentially with the well depths; and high NO_3^- concentrations were found in the wells with depths less than 50 m (Fig. 4b). High NO_3^- concentrations of groundwater were mainly located in alluvial plain (average 142 mg NO_3 L^{-1}), whereas groundwater NO_3^- concentrations were lower in the loess tableland (average 49 mg NO_3 L^{-1}) (Fig. 4c and d). A significant positive correlation was found between NO_3^- pollution percentage of wells and the proportion of orchard areas in cropland in each irrigated county (Fig. 5).

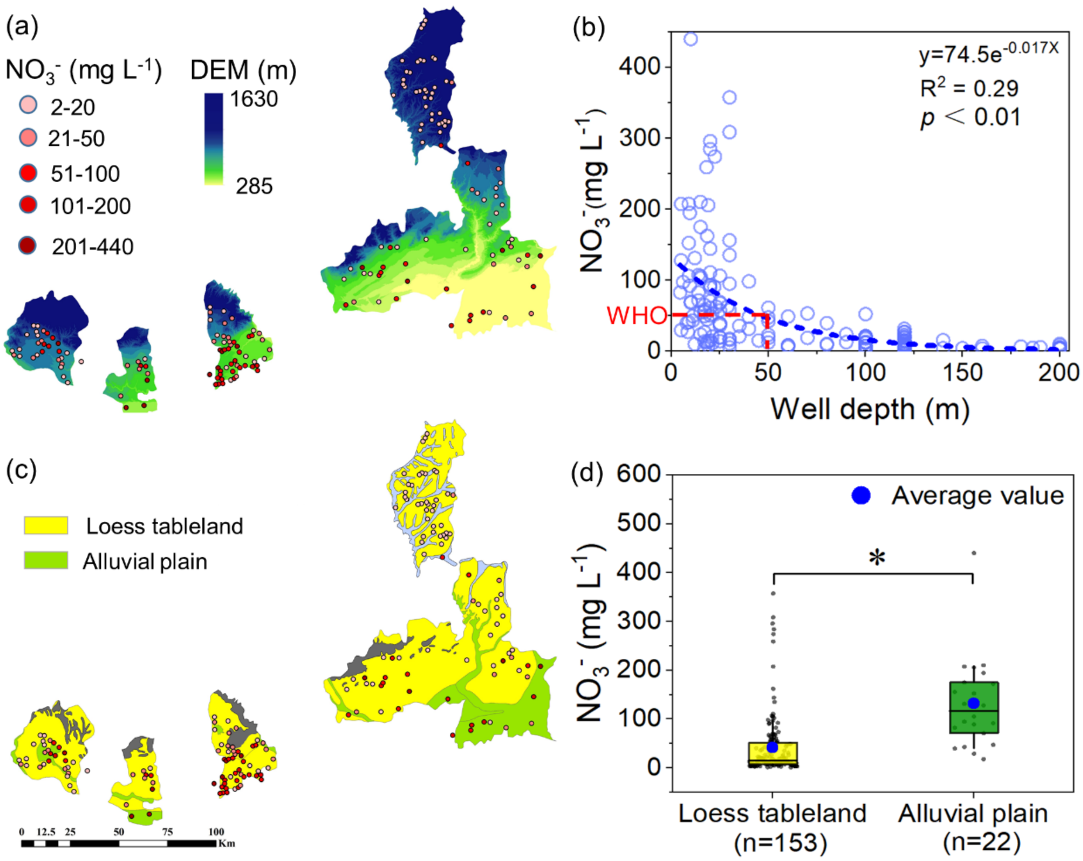

Fig. 4 Spatial variations of groundwater NO_3^- concentrations under different altitudes (a), well

depth (b) and geomorphology (c and d).

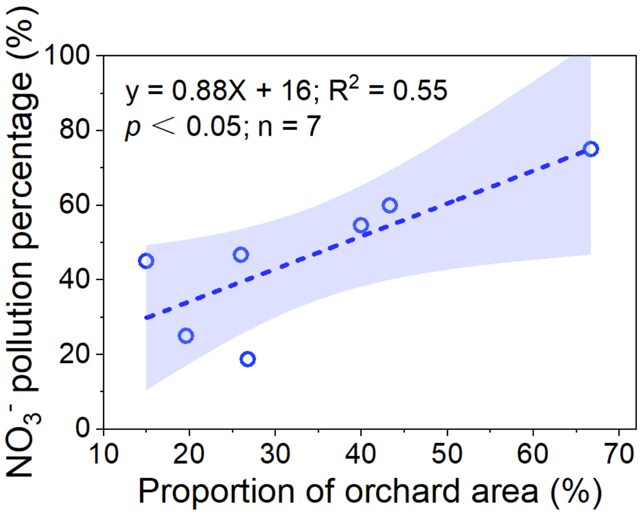

Fig. 5 The relationship between NO_3^- pollution percentage of well and the proportion of orchard area in cropland in each irrigated county. The area of each land-use type in each county was obtained from official statistics.

3.2.2 Temporal variations and drivers of groundwater NO_3^- concentration

Average groundwater NO_3^- concentrations of the shallow wells (depth less than 50 m) in all seasons followed the order of orchards > cereal lands ≈ residential area (Fig. 6). Average NO_3^- concentrations of groundwater in orchards and cereal lands gradually increased with time, and that in the residential area increased from the wet season (September 2020) to the dry season (March 2021) and then decreased from the dry season (March 2021) to the wet season (October 2021) (Fig. 6).

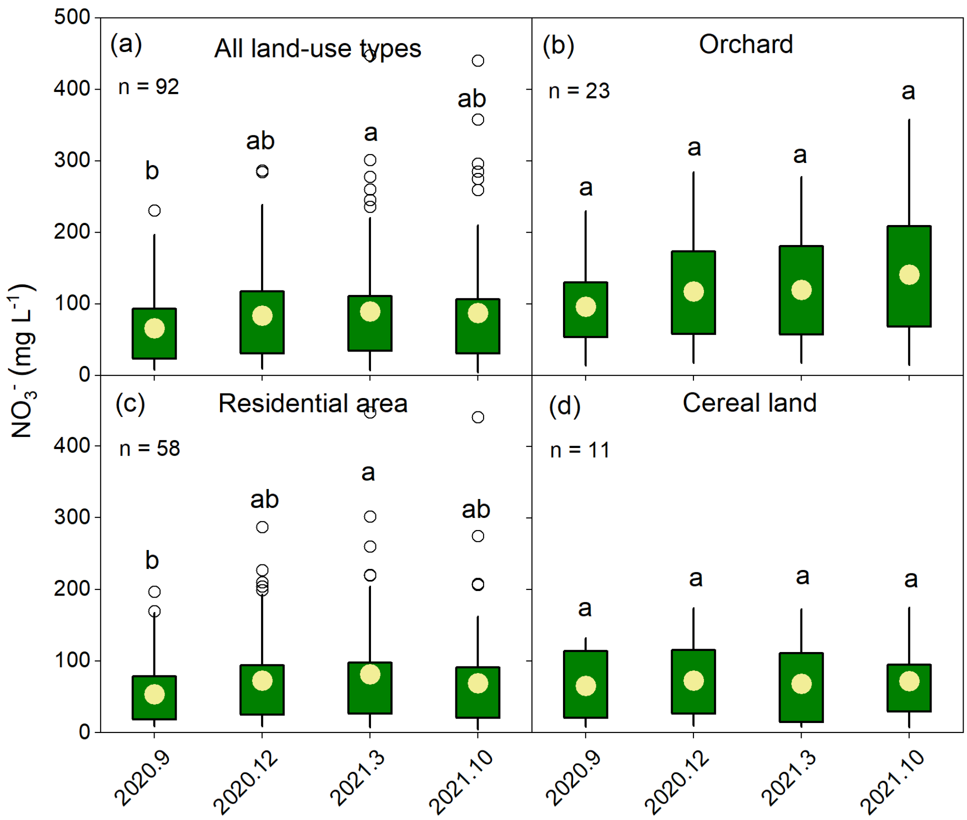

Fig. 6 Seasonal variations of groundwater NO_3^- concentrations in the shallow wells (depth less than 50 m) (a), and different land-use types, i.e., orchard (b), residential area (c) and cereal land (d). n means the number of groundwater samples, and the different lowercase letters (a and b) mean significant differences at the level of $p < 0.05$.

3.3 Vertical distribution and seasonal variations of NO_3^- in the vadose zone and aquifer

NO_3^- accumulations in the vadose zones of AO_1, AO_2 and AO_3 in the wet season were 15322 kg N ha^{-1}, 26583 kg N $ha^{-1}$and 16126 kg N ha^{-1}, respectively (Fig. S3). NO_3^- in the vadose zone of apple orchards has migrated to groundwater in the canal-irrigated region (Fig. 7). NO_3^- concentrations in deep vadose zones (74 mg NO_3 L^{-1}) were close to groundwater NO_3^- concentrations (69 mg NO_3 L^{-1}) in April 2021 (Dry season) (Fig. 7a), while NO_3^- concentrations at the bottom of the vadose zones during the wet season were much higher than groundwater NO_3^- concentrations from nearby monitoring wells resulting in a high NO_3^- concentration gradient in October 2021 (Fig. 7b, c and d). Compared to the soil profile of AO_1 in April 2021 (Fig. 7a), soil moisture contents in AO_1 in October 2021 were higher, the peak depth of NO_3^- migrated 2 m downward, and the water table rose by ~1 m (Fig. 7b).

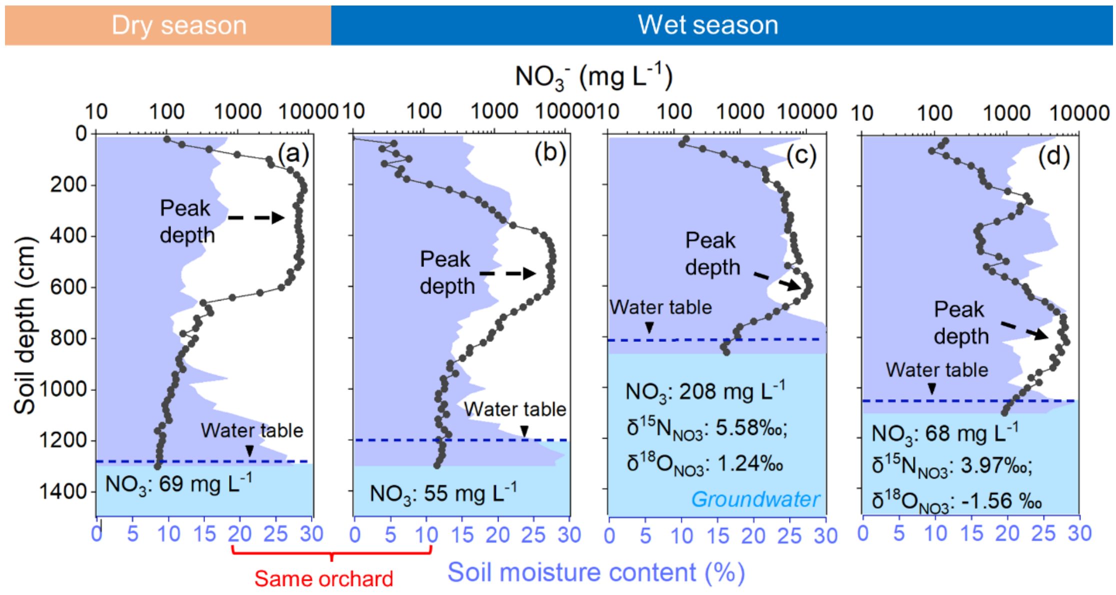

Fig. 7 NO_3^- and soil moisture contents in the vadose zones of three apple orchards i.e., AO_1 (a and b), AO_2 (b) and AO_3 (c), in the different seasons. The corresponding groundwater NO_3^- concentrations are from nearby monitoring wells, which are within 200 meters of the orchard sampling sites. The black dots represent NO_3^- concentrations of the soil water, and the blue shading indicates soil moisture content.

3.4 *Relationship of NO_3^- and Cl^-, isotopic composition of NO_3^- and SIAR analysis*

Groundwater samples from the dryland region mainly were plotted in the scope of soil N, and most of the groundwater samples from the irrigation region were distributed in the mixing region of fertilizer N, manure, soil N and sewage (Fig. 8a). The $\delta^{15}N$-NO_3^- and $\delta^{18}O$-NO_3^- values of groundwater in the study region ranged from -3‰ to +30‰ and from -2‰ to +20‰, respectively, and were mainly plotted in the overlapped area of "soil N", "NH_4^+ in fertilizer" and "Manure & Sewage" (Fig. 8b). A week positive correlation between $\delta^{15}N$-NO_3^- and NO_3^-

was observed with a correlation coefficient of 0.008 ($p > 0.05$; Fig. S2).

The results of SIAR mixing model analysis showed that there were obvious differences in the contribution ratios of the four potential NO_3^- sources in the dryland region and irrigated region (Fig. 9). The percentage contribution of NO_3^- sources for the dryland region was ranked as: NS (60.5%) > M (20%) > NF (17.8%) > AD (1.7%) (Fig. 9a), while that for irrigated was ranked: M (45.6%) > NS (39.9%) > NF (10.1%) > AD (4.4%).

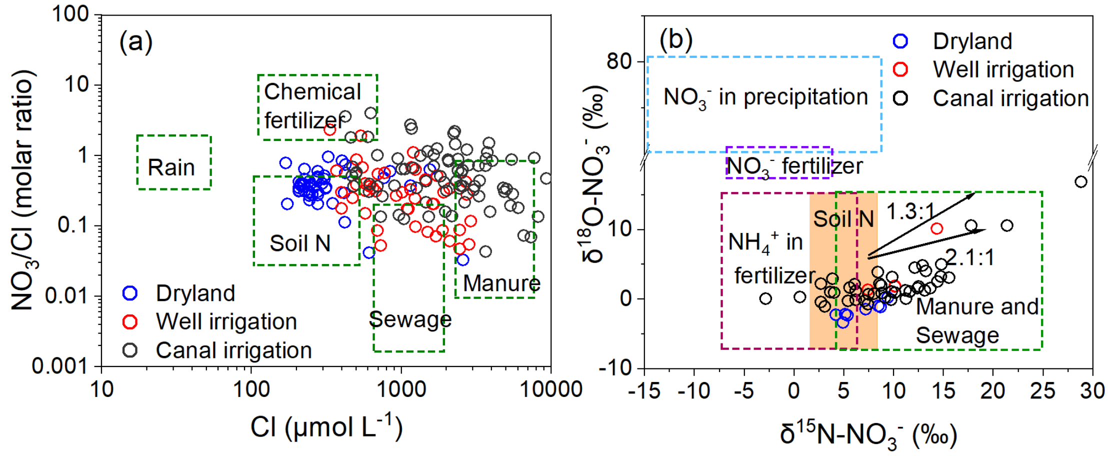

Fig. 8 Cross-plot of NO_3/Cl molar ratios and Cl values of groundwater (a), and the relationship between $\delta^{15}N$ and $\delta^{18}O$ of groundwater NO_3^- (b) in different regions. Data in (a) were adapted from (Meghdadi and Javar, 2018; Torres-Martínez *et al.*, 2021); the scopes of $\delta^{15}N$ and $\delta^{18}O$ for various sources were drawn according to Xue *et al.* (2009) and Kendall *et al.* (2007).

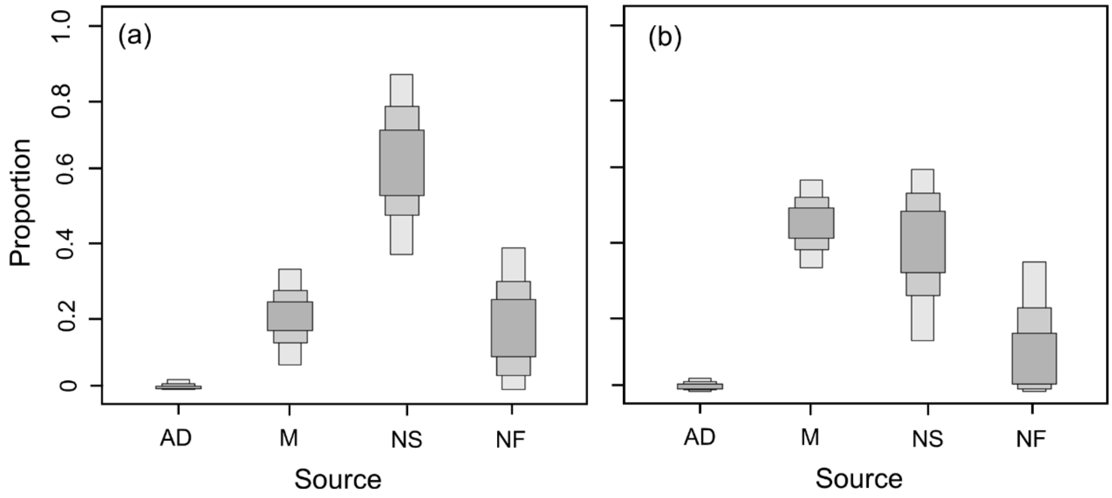

Fig. 9 Contribution proportion of different NO_3^- sources in the dryland region (a) and irrigated region (b). AD = atmospheric N deposition, NS = soil N, NF= chemical N fertilizer, and M = manure N.

4. Discussion

4.1 Spatial variations of groundwater NO_3^- concentration

Our study found that the NO_3^- concentrations of groundwater in dryland regions were lower than those in irrigated regions (Table 2). The SIAR analysis of dual isotopic of NO_3^- of groundwater in dryland regions also indicated that the nitrate in soil was mainly from the soil N stock (Fig. 9a). It indicates that the NO_3^- accumulated in soils of dryland region was mainly accumulated in the upper vadose zones due to the existence of dry layers in soil profiles of matured orchards (Zhu *et al.*, 2021; Zhu *et al.*, 2022b). The groundwater flow direction from dryland to irrigated regions avoids the effect of lateral groundwater flow on groundwater nitrate in dryland regions (Fig. S1). It is consistent with other studies at the dryland of the LP (Ma *et al.*, 2021). However, higher NO_3^- concentrations of groundwater were found in the irrigation region, the average concentration was 23 mg NO_3 L^{-1} in the well-irrigated region and 94 mg NO_3 L^{-1} in the canal-irrigated region (Table 2). The reason is that canal irrigation promotes the percolation of abundant NO_3^- from the vadose zone and consequent pollution of groundwater (Fig. 7), especially where the vadose zone is shallow. In addition, compared with the dryland region, the concentrations of Cl^-, SO_4^{2-}, NO_3^-, Ca^{2+} and Mg^{2+} ions in the irrigation regions were higher than that in the dryland region, and the hydrochemical types of the groundwater changed from HCO_3-Ca·Mg to SO_4·Cl·NO_3-Ca·Mg (Fig. 3). High Ca^{2+} and Mg^{2+} concentrations were primarily associated with the nitrification of ammonium-based or organic fertilizers (Aquilina *et al.*, 2012). Similar results have been founded in other intensive agricultural regions (Gao *et al.*, 2021a). This further indicates that the intensive agricultural practices (high fertilization, and irrigation) have significantly changed the biogeochemical process at the canal irrigation region.

The water table of the alluvial plain, which is located at low terrain areas (Fig. 4c), is close to the ground level, therefore, it responds fast to agricultural practices (irrigation and fertilization) and precipitation (Cameira *et al.*, 2021), thus having high NO_3^- groundwater concentrations. Groundwater NO_3^- pollution in low terrain areas is more serious in general due to groundwater lateral flow carrying upstream NO_3^-. Therefore, the apple-planting regions in the low-altitude loess tableland and alluvial plain irrigated by canals are NO_3^- vulnerable zones on the LP.

4.2 *Seasonal variations of groundwater NO_3^- concentration*

Significant seasonal differences of groundwater NO_3^- were found in the study region. NO_3^- concentrations in shallow wells showed an increasing trend from the wet season to the dry season (September 2020 - March 2021) (Fig. 6). It was often defined as the time lag (Basu *et al.*, 2022; Chen *et al.*, 2018; Wang *et al.*, 2013b). The time lag in this study can be attributed to high water input (irrigation and precipitation) in the wet season and NO_3^- vertical migration in the vadose zone, and NO_3^- lateral migration in the saturated zone (Fig. 7). On the one hand, deep soil layers in orchards keep a high moisture content in autumn due to the tree leaves fall causing low water consumption of apple trees. High soil moisture and nitrate contents in deep layers could continuously promote the NO_3^- migration from the vadose zone to aquifers. On the other hand, the high gradient of NO_3^- concentrations between the bottom of the vadose zone (600 mg NO_3 L^{-1} and 900 mg NO_3 L^{-1}) in the orchard and nearby groundwater (68 mg NO_3 L^{-1} and 208 mg NO_3 L^{-1}) (Fig. 7) further promote NO_3^- lateral migration in the saturated zone from orchard to residential area and cereal land causing groundwater NO_3^- concentration sustained growth from wet season to dry season (Fig. 6). In contrast, the time lag was shorter for orchard wells than that in residential wells because groundwater NO_3^- concentrations in orchards increased first and then stabilized, while that in the residential area continues to increase from the wet season (September 2020) to the dry season (March 2021) (Fig. 6b, c and d). This can be explained by the longer migration distance from the orchard to the residential area. Therefore, the period from the wet season to the dry season was the hot moment of groundwater NO_3^- pollution in the canal-irrigated region.

In addition, groundwater NO_3^- concentrations of shallow wells in the residential area decreased from the dry season (March 2021) to the wet season (October 2021), while the trend for orchards was the opposite, although not statistically significative (Fig. 6). This difference may be linked to the dilution effect that occurred in residential areas in irrigated regions due to the water table 1-2 m raising caused by rainfall vertical recharge groundwater and groundwater lateral recharge in this period (http://www.mwr.gov.cn) (Fig. 7b). The result partly agrees with Rotiroti *et al.* (2019) and Cameira *et al.* (2021), who reported that high groundwater recharge with low NO_3^- concentration can cause the dilution effect, thereby decreasing groundwater NO_3^- concentrations. The increase of NO_3^- concentration in orchard wells during the wet season could be caused by vadose zone nitrate deep migration accelerated by high groundwater recharge in this period (Fig. 7). Therefore, the nitrate accumulation profile in the vadose zones and dilution effect can jointly cause seasonal variations in regional groundwater NO_3^- concentrations.

4.3 Source identification of groundwater NO_3^-

The relations between Cl^- concentrations and NO_3^-/Cl^- ratios were used to identify the source of NO_3^-, such as fertilizer, soil organic N, manure and sewage, and precipitation (Meghdadi and Javar, 2018; Torres-Martínez *et al.*, 2021). Low Cl^- concentration and NO_3^-/Cl^- ratios of groundwater in dryland regions indicate that groundwater NO_3^- is mainly derived from soil organic N without the influence of synthetic N fertilizers. Groundwater samples in wells of the well and canal irrigated regions do not fit in the range of any specific source of NO_3^-, indicating that NO_3^- is derived from the mixing of fertilizer, soil organic N, and manure and sewage (Fig. 8a) (Torres-Martínez *et al.*, 2021). In addition, high Cl^- and SO_4^{2-} concentrations in groundwater were related to manure applicated in orchards accounting for 25% of annual N fertilizer input (Zhu *et al.*, 2022b; Wang *et al.*, 2013a).

Apart from human activities, isotopic compositions of NO_3^- are also altered by nitrification and denitrification (Gao *et al.*, 2021a). During the nitrification, the newly formed NO_3^- with one oxygen atom from the atmosphere O_2 and two oxygen atoms from the ambient water (Hollocher, 1984) leads to the $\delta^{18}O\text{-}NO_3^-$ values below 10‰ (Kendall, 1998; Böttcher *et al.*, 1990). The $\delta^{18}O\text{-}NO_3^-$ values of groundwater samples mostly fall in this range (Fig. 8b), indicating that the nitrification process is dominant in the study region. Microbial denitrification, which converts NO_3^- to gaseous N_2, results in $\delta^{18}O/\delta^{15}N$ ratios between 1:1.3 and 1:2.1 (Gao *et al.*, 2021a). The samples plotted do not show the denitrification trend meaning the absence of denitrification in groundwater (Fig. 8b). Relatively high (more than 2 mg L^{-1}) DO concentrations (between 3.2 mg L^{-1} and 9.6 mg L^{-1}, average 6.2 mg L^{-1}) in groundwater in the study region can limit denitrification process due to aerobic condition (Table 1) (Fukada *et al.*, 2003; Gao *et al.*, 2021b). This conclusion was also confirmed by the poor correlation (R^2= 0.008; p>0.05) between $\delta^{18}N$-NO_3^- values and NO_3^- concentrations (Fig. S2). Therefore, the denitrification process in aquifers was weak, indicating that it is difficult to improve the quality of groundwater once it is polluted.

Owing to the overlap of the isotope values of NO_3^-, it is difficult to recognize which source of NO_3^- is dominant in every region. SIAR mixing model was used to identify the main contributions of the four potential sources of NO_3^- in groundwater in the dryland and irrigated region, respectively (Fig. 9). In this study, the fractionation factor C_{jk} was set to 0 because the effect of denitrification can be ignored. The main contributing source of groundwater NO_3^- in dryland regions is NS (Fig. 9) due to the huge buffering effect of the thick vadose zone and the hinder effect of the dried soil layer protecting groundwater from agricultural activities (Zhu *et al.*, 2021). High manure and chemical fertilizers are applicated in the apple orchards (Wang et al., 2013a), this could explain the high contributing proportions (55.7%) of M&S and NF in the irrigation region (Fig. 9). The contribution of each NO_3^- source to the groundwater calculated using SIAR is in line with the results from the dual isotope analysis and the NO_3^-/Cl^- ratio method. In addition, the irrigation-water recharge alters the natural water cycle, raising groundwater levels at some locations and causing salt enrichment (such as Cl^-) under strong evaporation (Gao *et al.*, 2022), and further leading to a modification of the NO_3^-/Cl^- ratio method deviated from the scope of chemical N fertilizer in the irrigated region (Fig. 8a). The results may underestimate the contribution of fertilizer nitrogen, M&S and NF, and overestimate the contribution of NS, due to the overlap of the NO_3^- isotope values among NS, M&S and NF and high groundwater NO_3^- concentration in irrigated regions (Fig. 8). Overall, the results in the irrigated regions may underestimate the contributions of chemical N fertilizer. Therefore, the use of manure and chemical N fertilizers should be controlled in orchards to quickly reduce groundwater NO_3^- pollution.

4.4 *Implications and practical recommendations*

Converting cereal lands to apple orchards on the south of LP has caused serious NO_3^- pollution of regional groundwater due to the overuse of N fertilizers and flood irrigation. As a result, optimizing water and N fertilizer management is critical in the apple-planting regions in the south of LP. For example, reducing N fertilizer by 20-45% not only had no adverse effects on the yield and quality of fruit but also significantly reduced NO_3^- accumulation in the soil profile (Wang *et al.*, 2021; Lu *et al.*, 2018). Compared with flood irrigation, fertigation in orchards not only reduces the input of water and N, but also significantly reduces NO_3^- accumulation in soil and N leaching loss and increases N use efficiency (Phogat *et al.*, 2014). In addition, we argue that there is a need to designate NO_3^- vulnerable zones to preferentially and compulsively optimize water and N management of orchards to decrease NO_3^- leaching and its accumulation in the groundwater system.

The N balance (or N surplus) is often regarded as an indicator of N leaching loss for groundwater vulnerability assessment (Sela *et al.*, 2019; Tamagno *et al.*, 2022). However, the results in this study suggested high N surpluses do not always coincide with high groundwater NO_3^- concentrations, particularly in arid and semiarid regions with the thick unsaturated zone due to high N accumulation in the deep soil layers. Therefore, topography, vadose zone thickness, irrigation and seasonal rainfall should be considered comprehensively when evaluating groundwater pollution risks.

NO_3^- accumulation in the vadose zone slows N entering groundwater (Weitzman *et al.*, 2022), but a large legacy N in deep vadose zones will continuously provide NO_3^- to aquatic ecosystems, i.e., time lags, giving a challenge to groundwater protection (Fig. 7). In addition, improving NO_3^- dynamic monitoring in the vadose zone is a key to groundwater protection (Dahan, 2020), but the direct measurement of the NO_3^- migration in the thick unsaturated zone-aquifer system is too cumbersome and expensive on the LP. Numerical models are useful tools for simulating NO_3^- dynamic and quantifying NO_3^- travel time from the vadose zone to aquifers at the regional scale (Wang *et al.*, 2013b; Basu *et al.*, 2022). Therefore, it is urgent to develop a numerical model to simulate NO_3^- dynamic in the vadose zone by considering nitrate legacy and storage in the groundwater system, trying to guide the practices to achieve the desired water quality protection goal within the expected time scale.

5. Conclusion

Season-spatial variations and drivers of groundwater NO_3^- concentrations in the apple-planting regions on the Loess Plateau were assessed using NO_3^- distribution in the vadose zone, hydrochemical indicators and isotopic compositions in an integrated manner. Overuse of N fertilizers (manure and chemical N) and flood irrigation in apple orchards have caused a large NO_3^- accumulation in the deep vadose zone and groundwater nitrate pollution. Fertilizer N (manure and chemical fertilizer) is the main contributor to groundwater NO_3^- in the irrigation regions. A time lag of NO_3^- migration was found after the wet season leading to a steady increase in NO_3^- concentrations in groundwater. In this study, the canal-irrigated region, low-altitude loess tableland, and alluvial plain are hotspots of groundwater NO_3^- pollution, while the period from the wet season to the dry season was the hot moment of NO_3^- pollution in the canal-irrigated region. The NO_3^- vulnerable zones should be designated in the intensive apple-planting regions on the LP to mitigate groundwater NO_3^- pollution.

Acknowledgements

The authors thank the National Natural Science Foundation of China (No. 42277343), the National Key R&D Program of China (No. 2017YFD0200106), and the 111 Project (No. B12007) for the financial support.

References:

Aquilina, L., Poszwa, A., Walter, C., Vergnaud, V., Pierson-Wickmann, A. C., Ruiz, L., 2012. Long-term effects of high nitrogen loads on cation and carbon riverine export in agricultural catchments. *Environ.Sci.Technol.* 46(17): 9447-9455.

Basu, N. B., Van Meter, K. J., Byrnes, D. K., Van Cappellen, P., Brouwer, R., Jacobsen, B. H., Jarsjö, J., Rudolph, D. L., Cunha, M. C., Nelson, N., Bhattacharya, R., Destouni, G., Olsen, S. B., 2022. Managing nitrogen legacies to accelerate water quality improvement. *Nat. Geosci.* 15(2): 97-105.

Böttcher, J., Strebel, O., Voerkelius, S., Schmidt, H. L., 1990. Using isotope fractionation of nitrate-nitrogen and nitrate-oxygen for evaluation of microbial denitrification in a sandy aquifer. *J. Hydrol.* 114(3): 413-424.

Burow, K. R., Nolan, B. T., Rupert, M. G., Dubrovsky, N. M., 2010. Nitrate in groundwater of the United States, 1991− 2003. *Environ. Sci. Technol.* 44(13): 4988-4997.

Bryan, N.S., Loscalzo, J., 2011. Nitrite and nitrate in human health and disease. Humana Press, New York.

Cameira, M. d. R., Rolim, J., Valente, F., Mesquita, M., Dragosits, U., Cordovil, C. M. d. S., 2021. Translating the agricultural N surplus hazard into groundwater pollution risk: Implications for effectiveness of mitigation measures in nitrate vulnerable zones. *Agr. Ecosyst. Environ.* 306: 107204.

Cao, S., Fei, Y., Tian, X., Cui, X., Zhang, X., Yuan, R., Li, Y., 2021. Determining the origin and fate of nitrate in the Nanyang Basin, Central China, using environmental isotopes and the Bayesian mixing model. *Environ. Sci. Pollut. R.* 28(35): 48343-48361.

Chen, D., Shen, H., Hu, M., Wang, J., Zhang, Y., Dahlgren, R. A., 2018. Chapter Five - Legacy Nutrient Dynamics at the Watershed Scale: Principles, Modeling, and Implications. In *Advances in Agronomy*, Vol. 149, 237-313 (Ed D. L. Sparks). Academic Press.

Chen C. X., Liu Z. J., Chen Z. J., Zhou J. B., 2019. Characteristics of nitrate accumulation in soils of new and old apple orchards in Shaanxi Province. *Agricultural Research in the Arid Areas*, 2019, 37 (05): 171-175. (in Chinese with English abstract)

Dahan, O., 2020. Vadose zone monitoring as a key to groundwater protection. *Front. Water* 2: 599569.

Famiglietti, J. S., 2014. The global groundwater crisis. *Nat. Clim. Change* 4(11): 945-948.

FAOSTAT, 2019. Statistics Division. Food and Agriculture Organization of the United Nations. http://www.fao.org/faostat/en/#data.

Fukada, T., Hiscock, K. M., Dennis, P. F., Grischek, T., 2003. A dual isotope approach to identify denitrification in groundwater at a river-bank infiltration site. *Water Res.* 37(13): 3070-3078.

Gao, J., Li, Z., Chen, Z., Zhou, Y., Liu, W., Wang, L., Zhou, J., 2021a. Deterioration of groundwater quality along an increasing intensive land use pattern in a small catchment. *Agr. Water Manage.* 253: 106953.

Gao, J., Wang, S., Li, Z., Wang, L., Chen, Z., Zhou, J., 2021b. High nitrate accumulation in the vadose zone after land-use change from croplands to orchards. *Environ.Sci.Technol.* 55(9): 5782–5790.

Gao, Y., Chen, J., Qian, H., Wang, H., Ren, W., Qu, W., 2022. Hydrogeochemical characteristics and processes of groundwater in an over 2260 year irrigation district: A comparison between irrigated and nonirrigated areas. *J. Hydrol.* 606: 127437.

Gu, B. J., Ge, Y., Chang, S. X., Luo, W. D., Chang, J., 2013. Nitrate in groundwater of China: Sources and driving forces. *Global Environ. Chang.* 23(5): 1112-1121.

Hollocher, T. C., 1984. Source of the oxygen atoms of nitrate in the oxidation of nitrite by Nitrobacter agilis and evidence against a P-O-N anhydride mechanism in oxidative phosphorylation. *Arch. Biochem. Biophys.* 233(2): 721-727.

Huang, Y., Chang, Q., Li, Z., 2018. Land use change impacts on the amount and quality of recharge water in the loess tablelands of China. *Sci. Total Environ.* 628-629: 443-452.

Kendall, C., 1998. Tracing nitrogen sources and cycling in catchments. *Isotope Tracers in Catchment Hydrology*, 519-576.

Kendall, C., Elliott, E. M., Wankel, S. D., 2007. Tracing anthropogenic inputs of nitrogen to ecosystems. *Stable Isotopes in Ecology and Environmental Science*, 375-449.

Krug, F. J., Filho, H. B., Zagatto, E., Jrgensen, S. S., 1977. Rapid determination of sulphate in natural waters and plant digests by continuous flow injection turbidimetry. *The Analyst* 102(1216): 503.

Li, M., Guo, J., Xu, C., Lei, Y., Li, J., 2018. Identifying climatic factors and circulation indices related to apple yield variation in main production areas of China. *Glob. Ecol. Conserv.* 16: e00478.

Liu, Z. J., Ma, P. Y., Zhai, B. N., Zhou, J. B., 2019. Soil moisture decline and residual nitrate accumulation after converting cropland to apple orchard in a semiarid region: Evidence from the Loess Plateau. *Catena* 181: 104080.

Lu, Y. L., Kang, T. T., Gao, J. B., Chen, Z. J., Zhou, J. B., 2018. Reducing nitrogen fertilization of intensive kiwifruit orchards decreases nitrate accumulation in soil without compromising crop production. *J. Integr. Agr.* 17(6): 1421-1431.

Ma, B., Huang, T., Li, J., Li, Z., Long, Y., Zhang, F., Pang, Z., 2021. Tracing nitrate source and transformation in a semiarid loess aquifer with the thick unsaturated zone. *Catena* 198: 105045.

Meghdadi, A., Javar, N., 2018. Quantification of spatial and seasonal variations in the proportional contribution of nitrate sources using a multi-isotope approach and Bayesian isotope mixing model. *Environ. Pollut.* 235: 207-222.

Phogat, V., Skewes, M. A., Cox, J. W., Sanderson, G., Alam, J., Šimůnek, J., 2014. Seasonal simulation of water, salinity and nitrate dynamics under drip irrigated mandarin (Citrus reticulata) and assessing management options for drainage and nitrate leaching. *J. Hydrol.* 513: 504-516.

Rotiroti, M., Bonomi, T., Sacchi, E., McArthur, J. M., Stefania, G. A., Zanotti, C., Taviani, S., Patelli, M., Nava, V., Soler, V., Fumagalli, L., Leoni, B., 2019. The effects of irrigation on groundwater quality and quantity in a human-modified hydro-system: The Oglio River basin, Po Plain, northern Italy. *Sci. Total Environ.* 672: 342-356.

Sela, S., Woodbury, P. B., Marjerison, R., van Es, H. M., 2019. Towards applying N balance as a sustainability indicator for the US Corn Belt: realistic achievable targets, spatio-temporal variability and policy implications. *Environ. Res. Lett.* 14(6): 4015.

Sigman, D. M., Casciotti, K. L., Andreani, M., Barford, C., Galanter, M., Böhlke, J. K., 2001. A bacterial method for the nitrogen isotopic analysis of nitrate in seawater and freshwater. *Anal. Chem.* 73(17): 4145-4153.

Sörbo, B., 1987. Sulfate: Turbidimetric and nephelometric methods. *Method. Enzymol.* 143: 3-6.

Steffen, W., Richardson, K., Rockstrom, J., Cornell, S. E., Fetzer, I., Bennett, E. M., Biggs, R., Carpenter, S. R., de Vries, W., de Wit, C. A., Folke, C., Gerten, D., Heinke, J., Mace, G. M., Persson, L. M., Ramanathan, V., Reyers, B., Sorlin, S., 2015. Sustainability. Planetary boundaries: guiding human development on a changing planet. *Science* 347(6223): 1259855.

Tamagno, S., Eagle, A. J., McLellan, E. L., van Kessel, C., Linquist, B. A., Ladha, J. K., Pittelkow, C. M., 2022. Quantifying N leaching losses as a function of N balance: A path to sustainable food supply chains. *Agr. Ecosyst. Environ.* 324: 107714.

Torres-Martínez, J. A., Mora, A., Mahlknecht, J., Daesslé, L. W., Cervantes-Avilés, P. A., Ledesma-Ruiz, R., 2021. Estimation of nitrate pollution sources and transformations in groundwater of an intensive livestock-agricultural area (Comarca Lagunera), combining major ions, stable isotopes and MixSIAR model. *Environ. Pollut.* 269: 115445.

Van Meter, K. J., Van Cappellen, P., Basu, N. B., 2018. Legacy nitrogen may prevent achievement of water quality goals in the Gulf of Mexico. *Science* 360(6387): 427-430.

Wang, F., Ge, S., Lyu, M., Liu, J., Li, M., Jiang, Y., Xu, X., Xing, Y., Cao, H., Zhu, Z., Jiang, Y., 2021. DMPP reduces nitrogen fertilizer application rate, improves fruit quality, and reduces environmental cost of intensive apple production in China. *Sci. Total Environ.* 802: 149813.

Wang, X. Y., Tong, Y. A., Liu, F., Zhao, Z. P., 2013a. Evaluation of the situation of fertilization in apple fields in Shaanxi Province. *Journal of Plant Nutrition and Fertilizers* 19(1): 206–213. (in Chinese with English abstract)

Wang, L., Butcher, A. S., Stuart, M. E., Gooddy, D. C., Bloomfield, J. P., 2013b. The nitrate time bomb: a numerical way to investigate nitrate storage and lag time in the unsaturated zone. *Environ. Geochem. Hlth.* 35(5): 667-681.

Weitzman, J. N., Brooks, J. R., Compton, J. E., Faulkner, B. R., Mayer, P. M., Peachey, R. E., Rugh, W. D., Coulombe, R. A., Hatteberg, B., Hutchins, S. R., 2022. Deep soil nitrogen storage slows nitrate leaching through the vadose zone. *Agr. Ecosyst. Environ.* 332: 107949.

Willett, W., Rockström, J., Loken, B., Springmann, M., Lang, T., Vermeulen, S., Garnett, T., Tilman, D., DeClerck, F., Wood, A., Jonell, M., Clark, M., Gordon, L. J., Fanzo, J., Hawkes, C., Zurayk, R., Rivera, J. A., De Vries, W., Majele Sibanda, L., ... Murray, C. J. L., 2019. Food in the Anthropocene: the EAT–Lancet Commission on healthy diets from sustainable food systems. *The Lancet*, 393(10170), 447-492.

WHO (World Health Organization), 2011. Guidelines for Drinking Water Quality. In WHO Chronicle, 4th ed.; Vol. 38, pp. 104–108.

Xue, D., Botte, J., De Baets, B., Accoe, F., Nestler, A., Taylor, P., Van Cleemput, O., Berglund, M., Boeckx, P., 2009. Present limitations and future prospects of stable isotope methods for nitrate source identification in surface- and groundwater. *Water Res.* 43(5): 1159-1170.

Xue, D., De Baets, B., Van Cleemput, O., Hennessy, C., Berglund, M., Boeckx, P., 2012. Use of a Bayesian isotope mixing model to estimate proportional contributions of multiple nitrate sources in surface water. *Environ. Pollut.* 161: 43-49.

Zhu, X., Fu, W., Kong, X., Chen, C., Liu, Z., Chen, Z., Zhou, J., 2021. Nitrate accumulation in the soil profile is the main fate of surplus nitrogen after land-use change from cereal cultivation to apple orchards on the Loess Plateau. *Agr. Ecosyst. Environ.* 319: 107574.

Zhu, X., Zhou, P., Miao, P., Wang, H., Bai, X., Chen, Z., Zhou, J., 2022a. Nitrogen use and management in orchards and vegetable fields in China: Challenges and Solutions. *Front. Agr. Sci. Eng.* 9(3): 386–395.

Zhu, X., Miao, P., Wang, P., Zhang, S., Chen, Z., Zhou, J., 2022b. Variations and influencing factors of nitrate accumulation in the deep soil profiles of apple orchards on the Loess Plateau. *Agr. Ecosyst. Environ.* 335: 108005.

Zhu, Y., Jia, X., Shao, M., 2018. Loess thickness variations across the Loess Plateau of China. *Surv. Geophys.* 39(4): 715-727.

Ravindra, B., Subba Rao, N. & Dhanamjaya Rao, E.N. Groundwater quality monitoring for assessment of pollution levels and potability using WPI and WQI methods from a part of Guntur district, Andhra Pradesh, India. *Environ Dev Sustain* (2022).

Rao N S , Dinakar A , Kumari B K . Appraisal of vulnerable zones of non-cancer-causing health risks associated with exposure of nitrate and fluoride in groundwater from a rural part of India[J]. Environmental Research, 2021(2):111674.

Rao N S, Das R, Gugulothu S. Understanding the factors contributing to groundwater salinity in the coastal region of Andhra Pradesh, India[J]. Journal of Contaminant Hydrology, 2022, 250: 104053.

Xiao, J. , Lv, G. , Chai, N. , Hu, J. , & Jin, Z. . (2022). Hydrochemistry and source apportionment of boron, sulfate, and nitrate in the Fen River, a typical loess covered area in the eastern Chinese Loess Plateau. *Environmental Research*, 206, 112570-.